ISSN 1023-1935, Russian Journal of Electrochemistry, 2007, Vol. 43, No. 3, pp. 355–363. © Pleiades Publishing, Ltd. 2007.
Original Russian Text © T.A. Zotov, V.N. Verbetskii, T.Ya. Safonova, A.V. Garshev, O.A. Petrii, 2007, published in Elektrokhimiya, 2007, Vol. 43, No. 3, pp. 373–381.

SHORT COMMUNICATIONS

Hydrogen Sorption and Electrochemical Properties of Alloys: Systems Zr–Ti–Ni–V–Mn with Laves Phase Structures

T. A. Zotov, V. N. Verbetskii, T. Ya. Safonova, A. V. Garshev, and O. A. Petrii[z]

Moscow State University, Vorob'evy Gory 1, Moscow, 119992 Russia

Received March 16, 2006

Abstract—Using scanning electron microscopy and x-ray phase analysis techniques, it is shown that the C14-type Laves phase with a wide homogeneity reaching the $AB_{2.3}$ stoichiometry is the main phase in the $Zr_{0.5}Ti_{0.5}Ni_yV_{0.5}Mn_x$ alloys, where $y = 0.8–1.4$ and $x = 0.1–1.7$. With the increase in the nickel and manganese contents and in the stoichiometric ratio B/A, the hydrogen capacity decreases from 2 to 1.6 wt %, the equilibrium pressure of hydride phases increases, and the hydrides become less stable. The highest discharge capacity is reached for stoichiometric ratios $AB_{1.7–2.3}$, where the maximum discharge capacity at a discharge current density of 100 mA/g is 300 (mA h)/g. Alloys that contain ferrovanadium in place of vanadium are also considered.

DOI: 10.1134/S1023193507030147

Key words: intermetallic compounds, Laves phases, hydrogen sorption, metal-hydride electrodes, discharge capacity

INTRODUCTION

Although nickel–metal-hydride (Ni–MH) power sources are already produced commercially, their refinement is still a promising research direction. One of the ways for the improvement of the characteristics of Ni–MH batteries is the optimization of metal-hydride electrodes, which are manufactured, e. g., based on AB_2 alloys that have the Laves phase structure and exhibit the discharge capacity higher that the capacity of AB_5.

Alloys of the Zr–Ti–Ni–V–Mn system with the Laves phase structure are known to exhibit the hydrogen-sorption and electrochemical properties [1–9] adequate for their practical application. However, the results obtained by different authors on one and the same alloys of this system differ widely, because their properties depend strongly on the conditions of preparation, activation, and testing of MH electrodes. In particular, this makes it impossible to draw unambiguous conclusions on the effect of the alloy composition on its properties.

The major objective of this study is the elucidation of how the nickel and manganese contents affect the hydrogen-sorption and electrochemical properties of alloys of the Zr–Ti–Ni–V–Mn system in the homogeneity range of the Laves phase. Alloys $Zr_{0.5}Ti_{0.5}Ni_yV_{0.5}Mn_x$ with $x = 0.1–1.7$ and $y = 0.8–1.4$ were studied. Some of our results were published earlier in [11–14].

[z] Corresponding author, email: petrii@elch.chem.msu.ru

EXPRIMENTAL

Iodide titanium and zirconium (99.99%) and electrolytic vanadium, manganese, and nickel (99.9%) were used as the starting materials. Alloys were smelted in an arc furnace under an argon atmosphere. To achieve homogeneity, the samples were remelted 3–4 times. A small excess of manganese (~4 at %), which was determined experimentally, was added to compensate the melting loss. The homogenizing annealing was accomplished in vacuum-degassed quartz ampoules. Annealing was carried out for 240 h at 850°C. After the annealing, the alloys were quenched by immersing the ampoules in cold water. In total, 32 alloys were prepared and studied.

The alloy composition and homogeneity were monitored by means of an electron microscope LEO Supra 50VP (field-emission cathode). X-ray spectroscopic microanalysis was performed using an Oxford INCA Energy+ system (a Si(Li) detector with the resolution of 129 eV in the K_a Mn line of 5.894 eV).

The x-ray phase analysis of original alloys and their hydride phases was carried out using a URD-6 diffractometer with CuK_α radiation at $2\theta = 25–90°$ with 0.02° steps and 1- and 3-s exposure in each point.

Hydrogenation of samples and studies of their hydrogen-sorption properties were carried out on the Sieverts type set-up in the pressure range from 0.01 to 60 atm. The hydride composition was calculated based on the decrease in the hydrogen pressure after its reaction with an intermetallic compound (IMC). The pressure was measured by reference monometers of the

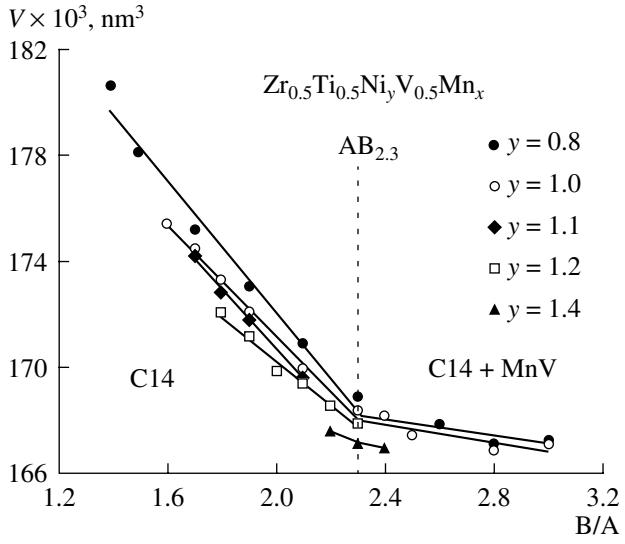

Fig. 1. Dependence of the unit cell volume of the C14 Laves phase on the ratio of A and B components of $Zr_{0.5}Ti_{0.5}Ni_yV_{0.5}Mn_x$ alloys.

0.4 grade of accuracy. The IMC reaction with hydrogen proceeded for 15–30 min. At its end, the pressure and the temperature were measured. The error of hydrogen content measurements was ±0.05 wt % H_2. For certain samples, equilibrium isotherms of hydrogen desorption were plotted on the coordinates pressure vs. hydride composition (PCT isotherms). The data for plotting hydrogen desorption isotherms were obtained by taking calibrated hydrogen portions from the working autoclave and transferring them to a vacuum-degassed buffer autoclave or a calibrated glass vessel of the vacuum-degassed set-up. In was assumed that the equilibrium in the system was reached if the pressure did not change for 30 min.

MH electrodes were prepared by pressing a powder mixture of 20% IMC and 80% copper under a pressure of 10 t/cm^2. An MH electrode represented a pellet of 7mm diameter and a mass of about 0.1 g with a hole in the center for fixing it to the current lead.

The electrochemical studies were carried out in a three-electrode electrochemical Pyrex cell with separated compartments, which contained a working MH electrode and a platinum counter electrode. A reversible hydrogen electrode (RHE, i.e. a Pt/Pt electrode in 6 M KOH solution) and a mercury-oxide electrode (–0.926 mV related to RHE) served as the reference electrodes. In this publication, all potentials (E) are referred to RHE. The electrolyte represented 6 M KOH. The procedures of charging and discharge of samples were carried out by means of a P-5827M potentiostat. The error in the discharge capacity measurements was ±7 (mA h)/g. In addition, a PC-governed automatic electronic galvanostat, a prototype of Potentiostat PS 7 OOO "Elins"[1] which provided measurements of the potential with the accuracy of ±0.02 mV and allowed maintaining the current with the accuracy of ±0.005 mA, was used. The error of discharge capacity measurements was below 5 (mA h)/g. Preliminary activation of electrodes consisted of their boiling (115°C) in 6 M KOH for 1.5 h. The activation conditions were optimized earlier [11–12]. The maximum discharge capacity was reached in 2–4 cycles. Samples were charged for 4–6 h at a current density of 100 mA/g. Hydrogen dissolved in the electrolyte was removed by bubbling argon through the working compartment of the cell. MH electrodes were discharged until a potential of 0.3 V was reached.

[1] http://elins.su.

EXPERIMENTAL RESULTS

Structure and Phase Composition of Original Alloys

The C14 Laves phase was the main phase of all samples studied. According to the data of electron-probe microanalysis and x-ray phase analysis, certain samples contained a small percentage (1–2 wt %) of a nonstoichiometric zirconium oxide phase (225, NaCl type) and an impurity (1–3 wt %) based on the (Ti, Zr)Ni phase (221, CsCl type, in alloys with y = 0.8, x = 0.6 and y = 1.0, x = 0.2, 0.3). As the manganese content in alloys increased up to x = 1.5, the MnV phase was formed and its content increased up to 10 wt %. Single-phase $Zr_{0.5}Ti_{0.5}Ni_yV_{0.5}Mn_x$ samples with the Laves phase structure existed at the ratio of A and B components not higher than $AB_{2.3}$. In the Laves phase homogeneity range, the volume of the C14 unit cell decreased with the increase in the manganese content and the B/A ratio (Fig. 1). Moreover, for samples with identical B/A ratios, the substitution of nickel for manganese resulted in the decrease in the C14 unit cell volume. Once the B/A ratio exceeded the ratio corresponding to $AB_{2.3}$ (Fig. 1), the curves charged their shape because the boundary of the homogeneity domain of the C14 phase was reached.

The refinement of diffraction profiles according to the Rietveld method was carried out only based on the model of static distribution of atoms between positions 2(a) and 6(h) of the B component in the C14 structure. The wide Laves phase region for $Zr_{0.5}Ti_{0.5}Ni_yV_{0.5}Mn_x$ alloys is explained by the redistribution of titanium and manganese atoms between A and B positions. In stoichiometric alloys (AB_2), the distribution of atoms in the C14 unit cell positions is described by the following scheme: component A = Zr + Ti; component B = Ni + V + Mn. In substoichiometric alloys (AB_n <2), Ti atoms (component A) partly occupy the B positions, viz., component A = Zr + Ti; component B = Ti + Ni + V + Mn. In superstoichiopmetric alloys (AB_n >2), manganese atoms (component B) partly occupy A positions, viz., component A = Zr + Ti + Mn; component B = Ni + V + Mn. Thus, the formula of the substoichiometric sample $Zr_{0.5}Ti_{0.5}Ni_{1.2}V_{0.5}Mn_{0.1}$ ($AB_{1.8}$) can be

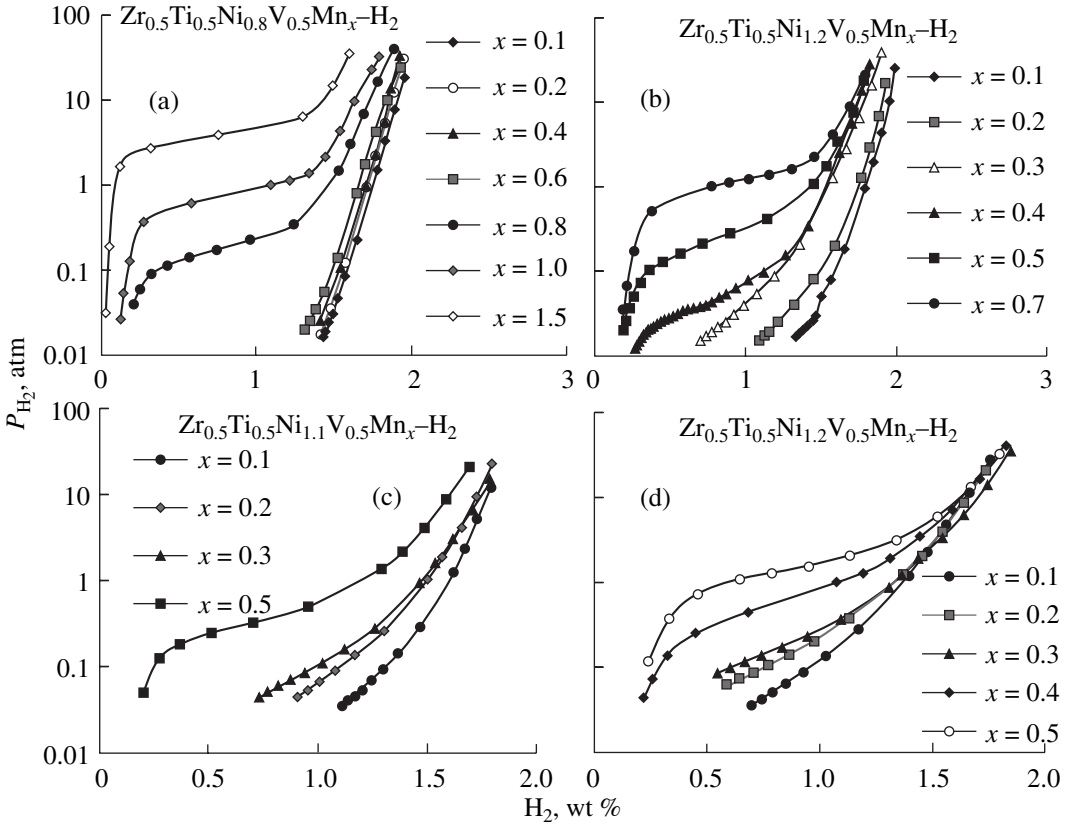

Fig. 2. Isotherm of hydrogen desorption in the system $Zr_{0.5}Ti_{0.5}Ni_yV_{0.5}Mn_x$–$H_2$, *y*: (a) 0.8, (b) 1.0, (c) 1.1, (d) 1.2 at room temperature.

presented in the stoichiometric (AB_2) form, namely, $(Zr_{0.54}Ti_{0.46})(Ti_{0.04}Ni_{0.64}V_{0.27}Mn_{0.05})_2$. For the superstoichiometric $Zr_{0.5}Ti_{0.5}Ni_{1.0}V_{0.5}Mn_{0.8}$ ($AB_{2.3}$) alloy, the formula is $Zr_{0.45}Ti_{0.45}Mn_{0.1}(Ni_{0.45}V_{0.23}Mn_{0.32})_2$.

Hydrogen Sorption Properties of Alloys

Figure 2 shows the isotherms of hydrogen desorption for samples $Zr_{0.5}Ti_{0.5}Ni_yV_{0.5}Mn_x$. Interaction with hydrogen was observed for 22 samples of 32. It was shown that under a pressure of up to 50 atm, only alloys with unit cell volumes larger than 0.1682 nm^3 sorbed hydrogen. Hydrogen absorption did not entailed changes in the metal matrix structure and was accompanied by the isotropic extension of the IMC lattice. The maximum hydrogen capacity of samples was in the interval of 1.6–2.0 wt %. Desorption isotherms did not have horizontal segments; this is why the equilibrium pressure of hydride dissociation was determined from the pressure that corresponded to the middle of the flattest segment in the curve.

An increase in the manganese content at a constant nickel content resulted in a decrease in the hydrogen-sorption capacity of samples (Table 1); however, this effect was small for high nickel contents. The increase in the manganese content in each series of alloys resulted in the increase in the dissociation pressure of hydrides and a decrease in the slope of the flat segment in hydrogen desorption isotherms. For alloys with the same B/A ratios, the substitution of nickel for manganese gave rise to an increase in the dissociation pressure and a decrease in the hydrogen capacity. The equilibrium dissociation pressure of the hydride phase increased with the decrease in the Laves phase lattice parameters. The changes in the enthalpy of hydrogen desorption ΔH were calculated according to the van't Hoff equation, where the dissociation pressure of IMC hydrides was taken at temperatures 0–90°C. With an increase in the contents of manganese and nickel, the enthalpy of hydrogen desorption decreased. The stability of hydride phases decreased with an increase in the unit cell volume of the Laves phase (Fig.1, Table 1).

Electrochemical Properties of Alloys

Figure 3 (curves *c* and *d* were measured in the automatic mode) shows the discharge curves of certain samples at a discharge current density of 100 mA/g. As was shown above, the maximum discharge capacity of samples was reached in 2–4 charge–discharge cycles. In the first cycle, ~90% of the maximum capacity was reached, which indirectly points to the effectiveness of the activation procedure chosen. In 10 charge–dis-

Table 1. Hydrogen sorption characteristics of alloys

Alloy composition	B/A	$\Delta V/V$[1], %	P_{H_2}[2], atm	H_2[3], wt %	H/IMC	H/M	ΔH_{des}, kJ/mol H_2
$Zr_{0.5}Ti_{0.5}Ni_{0.8}V_{0.5}Mn_{0.1}$	$AB_{1.4}$	17.9	<0.01	$1.96_{(18)}$	2.9(2)	1.2(2)	
$Zr_{0.5}Ti_{0.5}Ni_{0.8}V_{0.5}Mn_{0.2}$	$AB_{1.5}$	20.7	<0.01	$1.94_{(21)}$	3.0(1)	1.2(0)	
$Zr_{0.5}Ti_{0.5}Ni_{0.8}V_{0.5}Mn_{0.4}$	$AB_{1.7}$	19.0	<0.01	$1.94_{(37)}$	3.2(1)	1.1(9)	
$Zr_{0.5}Ti_{0.5}Ni_{0.8}V_{0.5}Mn_{0.6}$	$AB_{1.9}$	23.6	~0.02	$1.93_{(25)}$	3.4(1)	1.1(8)	41.6
$Zr_{0.5}Ti_{0.5}Ni_{0.8}V_{0.5}Mn_{0.8}$	$AB_{2.1}$	20.9	0.23	$1.89_{(40)}$	3.5(6)	1.1(5)	35.9
$Zr_{0.5}Ti_{0.5}Ni_{0.8}V_{0.5}Mn_{1.0}$	$AB_{2.3}$	–	0.76	$1.79_{(33)}$	3.5(8)	1.0(9)	32.3
$Zr_{0.5}Ti_{0.5}Ni_{0.8}V_{0.5}Mn_{1.5}$	$AB_{2.8}$	–	4.0	$1.60_{(36)}$	3.6(3)	0.9(5)	28.2
$Zr_{0.5}Ti_{0.5}Ni_{1.0}V_{0.5}Mn_{0.1}$	$AB_{1.6}$	–	<0.01	$1.94_{(26)}$	3.1(2)	1.2(0)	49.1
$Zr_{0.5}Ti_{0.5}Ni_{1.0}V_{0.5}Mn_{0.2}$	$AB_{1.7}$	–	~0.02	$1.91_{(17)}$	3.1(8)	1.1(8)	
$Zr_{0.5}Ti_{0.5}Ni_{1.0}V_{0.5}Mn_{0.3}$	$AB_{1.8}$	18.7	~0.04	$1.90_{(40)}$	3.2(8)	1.1(7)	39.8
$Zr_{0.5}Ti_{0.5}Ni_{1.0}V_{0.5}Mn_{0.4}$	$AB_{1.9}$	–	0.065	$1.82_{(29)}$	3.2(3)	1.1(1)	37.8
$Zr_{0.5}Ti_{0.5}Ni_{1.0}V_{0.5}Mn_{0.6}$	$AB_{2.1}$	–	0.26	$1.79_{(18)}$	3.3(8)	1.0(9)	35.6
$Zr_{0.5}Ti_{0.5}Ni_{1.0}V_{0.5}Mn_{0.8}$	$AB_{2.3}$	–	1.13	$1.79_{(22)}$	3.5(9)	1.0(9)	30.7
$Zr_{0.5}Ti_{0.5}Ni_{1.1}V_{0.5}Mn_{0.1}$	$AB_{1.7}$	18.4	~0.03	$1.81_{(22)}$	2.9(9)	1.1(2)	41.8
$Zr_{0.5}Ti_{0.5}Ni_{1.1}V_{0.5}Mn_{0.2}$	$AB_{1.8}$	19.9	0.04	$1.80_{(22)}$	3.1(0)	1.1(1)	37.7
$Zr_{0.5}Ti_{0.5}Ni_{1.1}V_{0.5}Mn_{0.3}$	$AB_{1.9}$	19.7	0.09	$1.83_{(15)}$	3.2(6)	1.1(2)	36.9
$Zr_{0.5}Ti_{0.5}Ni_{1.1}V_{0.5}Mn_{0.5}$	$AB_{2.1}$	–	0.32	$1.71_{(21)}$	3.23	1.04	35.3
$Zr_{0.5}Ti_{0.5}Ni_{1.2}V_{0.5}Mn_{0.1}$	$AB_{1.8}$	17.0	0.043	$1.76_{(28)}$	3.0(3)	1.0(8)	37.2
$Zr_{0.5}Ti_{0.5}Ni_{1.2}V_{0.5}Mn_{0.2}$	$AB_{1.9}$	17.6	0.14	$1.74_{(21)}$	3.1(0)	1.0(8)	36.1
$Zr_{0.5}Ti_{0.5}Ni_{1.2}V_{0.5}Mn_{0.3}$	AB_2	18.5	0.24	$1.72_{(16)}$	3.1(5)	1.0(5)	35.1
$Zr_{0.5}Ti_{0.5}Ni_{1.2}V_{0.5}Mn_{0.4}$	$AB_{2.1}$	17.6	0.64	$1.83_{(40)}$	3.1(9)	1.0(3)	33.7
$Zr_{0.5}Ti_{0.5}Ni_{1.2}V_{0.5}Mn_{0.5}$	$AB_{2.2}$	17.1	1.58	$1.80_{(32)}$	3.2(3)	1.0(1)	30.3

[1] Relative change in the C14 unit cell volume at hydrogenation: $100\%(V_{IMC\text{-}H} - V_{IMC})/V_{IMC}$.
[2] Equilibrium dissociation pressure of the hydride phase at room temperature.
[3] Weight content of hydrogen at a pressure P, atm (shown in parentheses), H/IMC is the number of hydrogen atoms per alloy formula unit, H/M = (H/IMC)/(1 + (B/A)).

charge cycles, no decrease in the discharge capacity was observed.

The potential of a MH electrode in the charged state was established in a range from 0 to –30 mV (Fig. 3) and gradually approached 0. The reasons for the establishment of negative potentials require special studies. Probably, this points to the accumulation of certain amounts of molecular hydrogen in the electrode material during its polarization in the potential range of evolution of molecular hydrogen, which is followed by its slow removal. Negative rest potentials were observed earlier for ZrNi alloys [15]. Note that the data on the determination of discharge capacities of IMC suggest that the equilibrium between hydrogen in the IMC and in the solution is established slowly, which should be taken into account when comparing the data of gas-phase and electrochemical measurements. In the equilibrium state, the hydrogen pressure (P_0) in the electrode calculated according to the Nernst equation should be ~1–9 atm (Table 2). However, the potential value also depends on the corrosion processes. Hence, the elucidation of the nature of rest potentials requires studying the corrosion behavior of IMC. Thus, the hydrogen content in the alloy of a MH electrode somewhat exceeds the hydrogen capacity of alloys corresponding to a pressure of 1 atm; however, this deviation is small as follows from Fig. 3. The hydrogen capacity of alloys, which was determined in the gas-phase experiments at pressures corresponding to the electrochemical measurements of rest potentials, was expressed in (mA h)/g and designated below as C^*. This capacity termed as the effective capacity decreased with the increase in the manganese and nickel contents (Table 2).

Dissociation pressures of hydride phases in the vicinity of the plateau in the discharge curves were determined (Table 2). The dissociation pressures of hydrides measured under dynamic conditions of electrochemical experiments were substantially lower than the equilibrium pressures of hydride dissociation (compare Tables 1 and 2). Moreover, it was found that the slopes of isotherms of hydrogen desorption plotted

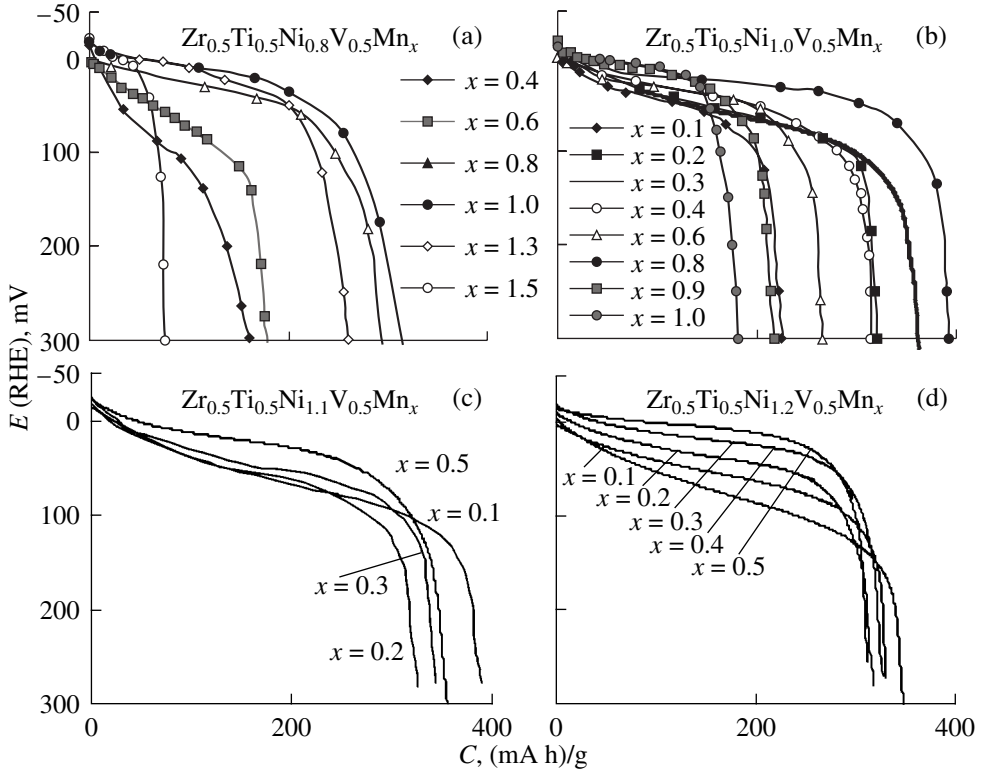

Fig. 3. Discharge curves of $Zr_{0.5}Ti_{0.5}Ni_yV_{0.5}Mn_x$ samples at room temperature and a discharge current density of 100 mA/g.

based on discharge curves always exceeded those of equilibrium gas-phase isotherms and the plateau slope decreased with the increase in the B/A ratio of alloys, just as for gas-phase isotherms. The analysis of electrochemical isotherms of hydrogen desorption has shown that for alloys with the same stoichiometric ratios, the plateau slope decreased with the increase in the nickel content. Thus, the smallest deviation from the equilibrium conditions at the electrochemical discharge was observed for nickel-rich alloys.

For hydrogen sorbing samples $Zr_{0.5}Ti_{0.5}Ni_yV_{0.5}Mn_x$, a linear dependence of the discharge capacity on the discharge current density was observed for i = 100–600 mA/g. Linear extrapolation to i = 0 mA/g allowed us to obtain the effective limiting discharge capacity C_0 (Table 2). The discharge stability for samples $Zr_{0.5}Ti_{0.5}Ni_yV_{0.5}Mn_x$ was calculated as a ratio of the discharge capacity at a current density of 400 mA/g to C_0, i.e. $100\% \cdot C_{400}/C_0$ (Table 2).

DISCUSSION

Figure 4 shows the dependences of the discharge capacity measured under electrochemical conditions and of C^* on the manganese content and the B/A ratio in alloys. The dependences have intricate nonmonotonic shapes and strongly differ from those expected based on the gas-phase measurements. The presence of minimums and maximums in the discharge capacity vs. B/A ratio dependences is associated with the opposite effects of two different factors, namely, the hydride phase stability and the electrocatalytic activity of materials. Indeed, the electrochemical discharge includes the following stages: the hydrogen transport from the bulk of IMC hydride grains to the electrode surface, the transition of absorbed hydrogen into adsorbed hydrogen, and the hydrogen ionization.

The rate of the first stage is determined by the hydrogen diffusion in the IMC hydride bulk. In the literature [16–18], it was shown that the decrease in the stability of hydride phases entails the acceleration of hydrogen diffusion. For samples $Zr_{0.5}Ti_{0.5}Ni_yV_{0.5}Mn_x$, the stability of hydride phases decreases with the increase in x for each y (Table 2); hence, the diffusion rate can increase with the increase in the B/A ratio. The rates of other two stages are determined by the electrocatalytic activity of the MH electrode material, which depends on the pretreatment conditions. Activation in hot alkali results in the formation of a surface layer enriched in nickel, which plays the role of a catalyst in the electrochemical reaction of IMC with hydrogen [10]. With an increase in the manganese content in each series of studied alloys, the concentrations of the other metals including nickel decrease. Hence, for the same duration of the alkali treatment, the nickel content in the catalytic surface layer of alloys will decrease with an increase in the manganese content. These factors can be the reason for the different behavior of alloys in the

Table 2. Discharge characteristics of $Zr_{0.5}Ti_{0.5}Ni_yV_{0.5}Mn_x$ alloys

Alloy composition	B/A	$E_{(RHE)}$[1], mV	P_{H_2}[2], atm	C^*, (mA h)/g	C_0[3], (mA h)/g	C_{100}[4], (mA h)/g	C_{400}, (mA h)/g	Discharge stability,[5] %
$Zr_{0.5}Ti_{0.5}Ni_{0.8}V_{0.5}Mn_{0.1}$	$AB_{1.4}$	–	–	496	25	21	5	20
$Zr_{0.5}Ti_{0.5}Ni_{0.8}V_{0.5}Mn_{0.2}$	$AB_{1.5}$	–	–	487	141	127	50	36
$Zr_{0.5}Ti_{0.5}Ni_{0.8}V_{0.5}Mn_{0.4}$	$AB_{1.7}$	87	0.001	487	180	160	53	29
$Zr_{0.5}Ti_{0.5}Ni_{0.8}V_{0.5}Mn_{0.6}$	$AB_{1.9}$	50	0.02	471	200	178	58	29
$Zr_{0.5}Ti_{0.5}Ni_{0.8}V_{0.5}Mn_{0.8}$	$AB_{2.1}$	28	0.11	435	345	296	153	44
$Zr_{0.5}Ti_{0.5}Ni_{0.8}V_{0.5}Mn_{1.0}$	$AB_{2.3}$	10	0.45	405	370	315	145	39
$Zr_{0.5}Ti_{0.5}Ni_{0.8}V_{0.5}Mn_{1.3}$	$AB_{2.6}$	0	1.0		300	258	128	43
$Zr_{0.5}Ti_{0.5}Ni_{0.8}V_{0.5}Mn_{1.5}$	$AB_{2.8}$	–6	1.61	107	80	77	70	88
$Zr_{0.5}Ti_{0.5}Ni_{0.8}V_{0.5}Mn_{1.7}$	$AB_{3.0}$	–	–		67	65	63	94
$Zr_{0.5}Ti_{0.5}Ni_{1.0}V_{0.5}Mn_{0.1}$	$AB_{1.6}$	76	0.003	492	250	240	120	48
$Zr_{0.5}Ti_{0.5}Ni_{1.0}V_{0.5}Mn_{0.2}$	$AB_{1.7}$	53	0.015	479	340	318	255	75
$Zr_{0.5}Ti_{0.5}Ni_{1.0}V_{0.5}Mn_{0.3}$	$AB_{1.8}$	48	0.023	450	385	360	288	75
$Zr_{0.5}Ti_{0.5}Ni_{1.0}V_{0.5}Mn_{0.4}$	$AB_{1.9}$	42	0.035	442	325	312	279	86
$Zr_{0.5}Ti_{0.5}Ni_{1.0}V_{0.5}Mn_{0.6}$	$AB_{2.1}$	30	0.092	434	280	262	217	78
$Zr_{0.5}Ti_{0.5}Ni_{1.0}V_{0.5}Mn_{0.8}$	$AB_{2.3}$	22	0.173	415	415	391	324	78
$Zr_{0.5}Ti_{0.5}Ni_{1.0}V_{0.5}Mn_{0.9}$	$AB_{2.4}$	8	0.53		215	215	212	99
$Zr_{0.5}Ti_{0.5}Ni_{1.0}V_{0.5}Mn_{1.0}$	$AB_{2.5}$	5	0.67		180	178	176	98
$Zr_{0.5}Ti_{0.5}Ni_{1.1}V_{0.5}Mn_{0.1}$	$AB_{1.7}$	66	0.005	457	405	389	336	83
$Zr_{0.5}Ti_{0.5}Ni_{1.1}V_{0.5}Mn_{0.2}$	$AB_{1.8}$	55	0.011	438	332	323	295	89
$Zr_{0.5}Ti_{0.5}Ni_{1.1}V_{0.5}Mn_{0.3}$	$AB_{1.9}$	49	0.02	441	350	339	320	91
$Zr_{0.5}Ti_{0.5}Ni_{1.1}V_{0.5}Mn_{0.5}$	$AB_{2.1}$	20	0.20	389	363	355	325	90
$Zr_{0.5}Ti_{0.5}Ni_{1.2}V_{0.5}Mn_{0.1}$	$AB_{1.8}$	59	0.009	405	364	350	305	84
$Zr_{0.5}Ti_{0.5}Ni_{1.2}V_{0.5}Mn_{0.2}$	$AB_{1.9}$	50	0.016	413	345	335	307	89
$Zr_{0.5}Ti_{0.5}Ni_{1.2}V_{0.5}Mn_{0.3}$	$AB_{2.0}$	32	0.076	405	322	318	310	96
$Zr_{0.5}Ti_{0.5}Ni_{1.2}V_{0.5}Mn_{0.4}$	$AB_{2.1}$	15	0.30	383	330	327	319	97
$Zr_{0.5}Ti_{0.5}Ni_{1.2}V_{0.5}Mn_{0.5}$	$AB_{2.2}$	1.0	0.90	356	321	320	314	98

[1] Potential in the middle of a flat segment in the discharge curve with respect to the reversible hydrogen electrode in the same solution.
[2] Dissociation pressure of the hydride phase calculated from $E_{(RHE)}$.
[3] Conditional limiting discharge capacity (see text).
[4] Discharge capacity at a discharge current density of 100 mA/g (C_{100}) and 400 mA/g (C_{400}).
[5] Discharge stability, 100% C_{400}/C_0.

gas phase and in electrolyte solutions. Probably, the data on the electrochemical desorption of hydrogen under equilibrium conditions could be helpful for more comprehensive understanding of the nature of these differences. On the whole, the higher the nickel content in an IMC the better the correspondence between the gas-phase and electrochemical results.

Figure 5 illustrates the dependence of the discharge capacity at a current density of 100 mA/g on the composition of $Zr_{0.5}Ti_{0.5}Ni_yV_{0.5}Mn_x$ alloys. Compositions with close electrochemical characteristics correspond to the same symbols. It is evident that the probability of obtaining an alloy with a high discharge capacity is the highest in the range of compositions from $AB_{1.7}$ to

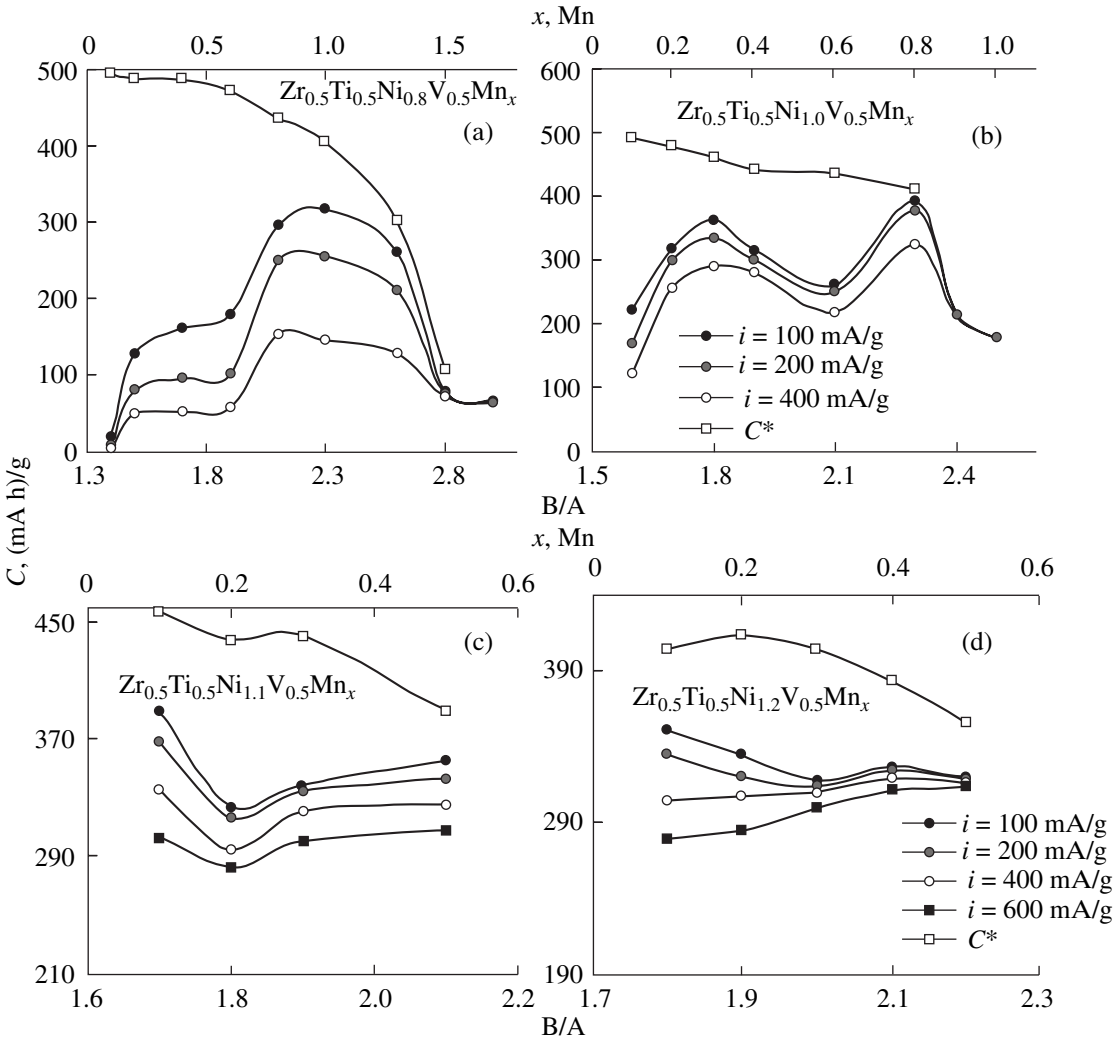

Fig. 4. Reference discharge capacities (C^*) and discharge capacities at different current densities for $Zr_{0.5}Ti_{0.5}Ni_yV_{0.5}Mn_x$ samples as a function of the manganese content and the ration of A and B components.

$AB_{2.3}$ for y = 1.0–1.2 and x = 0.1–0.6. In Fig. 5, this region is confined by dashed lines. Once y increases to 1.4 or decreases to 0.8, the discharge capacity substantially decreases.

As regards the discharge capacity and the discharge stability, the best samples were $Zr_{0.5}Ti_{0.5}Ni_{1.0}V_{0.5}Mn_{0.3}$ (360_{100}, 75%), $Zr_{0.5}Ti_{0.5}Ni_{1.0}V_{0.5}Mn_{0.8}$ (391_{100}, 78%), $Zr_{0.5}Ti_{0.5}Ni_{1.1}V_{0.5}Mn_{0.1}$ (389_{100}, 83%), $Zr_{0.5}Ti_{0.5}Ni_{1.1}V_{0.5}Mn_{0.5}$ (355_{100}, 90%), and $Zr_{0.5}Ti_{0.5}Ni_{1.2}V_{0.5}Mn_{0.1}$ (350_{100}, 84%). The discharge capacity of these samples exceeds the capacity of a commercial alloy of the AB_5 type by 30–35%. It is possible that the electrochemical properties of samples studied in this work can be improved by optimizing the procedure of preparation and treatment of MH electrodes by taking into account the individual properties of alloys.

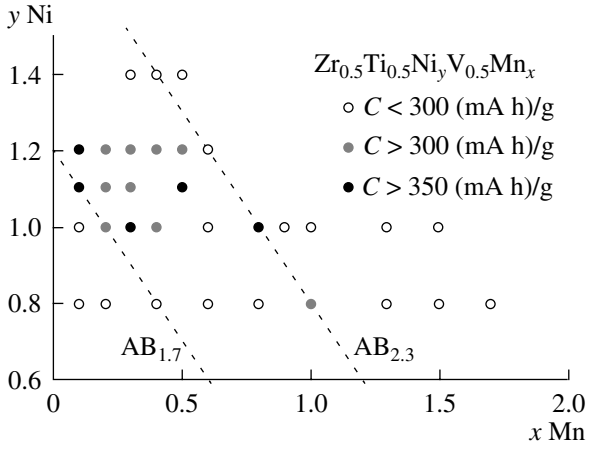

Fig. 5. Schematic diagram of the dependence of the discharge capacity at a current density of 100 mA/g on the composition of $Zr_{0.5}Ti_{0.5}Ni_yV_{0.5}Mn_x$ alloys.

Table 3. Properties of $Zr_{0.5}Ti_{0.5}Ni_y(FeV)_{0.5}Mn_x$ alloys

Alloy composition	B/A	Phase composition	P_{H_2} [1], atm	H_2 [2], wt %	C*, (mA h)/g	C_{100}, (mA h)/g
$Zr_{0.5}Ti_{0.5}Ni_{1.0}V_{0.3}Fe_{0.2}Mn_{0.1}$	$AB_{1.6}$	C14 89% (TiZr)Ni 8% ZrO_x 3%	0.25	1.4(9)	364	236
$Zr_{0.5}Ti_{0.5}Ni_{1.0}V_{0.3}Fe_{0.2}Mn_{0.2}$	$AB_{1.7}$	C14 91% (TiZr)Ni 5% ZrO_x 4%	0.5	1.4(4)	340	247
$Zr_{0.5}Ti_{0.5}Ni_{1.0}V_{0.3}Fe_{0.2}Mn_{0.3}$	$AB_{1.8}$	C14 93% (TiZr)Ni 4% ZrO_x 3%	1.0	1.3(9)	318	300

[1] Equilibrium dissociation pressure of the hydride phase at room temperature.
[2] Hydrogen content in the alloy at 10 atm.

Properties of $Zr_{0.5}Ti_{0.5}Ni_yFe_{0.2}V_{0.3}Mn_x$ Samples

Electrolytic vanadium (VEL) is the most expensive component in the alloys studied. This is why the next stage of our study was the elucidation of the possibility of substitution of a technological alloy, namely, ferrovanadium, for vanadium. We used ferrovanadium 50 which contained 52.5 wt % V. The substitution was carried out for those alloys, which demonstrated low pressures of the hydride phase dissociation and high hydrogen contents. The studies of alloys containing ferrovanadium did not involve any homogenizing annealing.

The substitution of ferrovanadium for vanadium resulted in a decrease in the lattice parameter of the Laves phase and the formation of a substantial amount of a secondary phase with the cubic lattice. The hydrogen content decreased and the dissociation pressure increases as compared with unsubstituted alloys (Table 3).

The substitution of ferrovanadium for vanadium also led to a decrease in the discharge capacity. For alloys with ferrovanadium, the discharge capacity increased with the increase in the manganese content, just as for vanadium alloys (compare Tables 2 and 3). The sample $Zr_{0.5}Ti_{0.5}Ni_{1.0}V_{0.3}Fe_{0.2}Mn_{0.3}$ had the maximum discharge capacity (~300_{100} (mA h)/g), which is comparable with the capacity of commercial AB_5 alloys.

CONCLUSIONS

The structure of the $Zr_{0.5}Ti_{0.5}Ni_yV_{0.5}Mn_x$ alloys was studied by electron microscopy, electron-probe microanalysis, and x-ray phase analysis techniques. It was shown that the C14 Laves phase has a homogeneity region at a ratio of A and B components $B/A_{\leq 2.3}$. Studies of the hydrogen interaction with $Zr_{0.5}Ti_{0.5}Ni_yV_{0.5}Mn_x$ alloys have shown that the hydrogen content is 1.6–2.0 wt % and the increase in the nickel and manganese contents results in the decrease in the hydrogen capacity and the stability of IMC hydrides. The alloys that demonstrated the highest discharge characteristics lie in the composition region between $AB_{1.7}$ and $AB_{2.3}$ with the nickel and manganese contents in the intervals of 29–42 at % and 4–24 at %, respectively. Some of the alloys, which exhibited the highest discharge capacity, can be recommended for practical application as the electrodes in Ni–MH batteries. The discharge capacity value found for the $Zr_{0.5}Ti_{0.5}Ni_{1.0}V_{0.3}Fe_{0.2}Mn_{0.3}$ alloy that contained ferrovanadium (~300 (mA h)/g) is comparable with the capacity of a conventional MH electrodes based on AB_5-type IMC.

REFERENCES

1. Petrii, O.A., Vasina, S.Ya, and Korobov, I.I., *Usp. Khim.*, 1996, vol. 65, p. 195.
2. Kleperis, J., Wójcik, G., Czerwinski, A., Skowronski, J., Kopczyk, M., and Beltowska-Brzezinska, M., *J. Solid State Electrochem.*, 2001, vol. 5, p. 229.
3. Semykin, A.V. and Kazarinov, I.A., *Elektrokhim. Energ.*, 2004, vol. 4, pp. 3, 63, 113.
4. Kazarinov, I.A. and Semykin, A.V., *Elektrodnye materialy na osnove gidridov i splavov* (The Electrode Materials Based on Hydrides and Alloys), Saratov: Saratov. Gos. Univ., 2005.
5. Lee, H.-H., Lee, K.-Y., and Lee, J.-Y., *J. Alloys Comp.,* 1997, vol. 253-254, p. 601.
6. Kim., J.-S., Paik, C.H., Cho, W.I., Cho, B.W., Yun, K.S., and Kim, S.J., *J. Power Sources*, 1998, vol. 75, p. 1.
7. Kim, D.-M., Jeon, S.-W., and Lee, J.-Y., *J. Alloys Comp.*, 1998, vol. 279, p. 209.

8. Kim, D.-M., Lee, H., Cho, K., and Lee, J.-Y., *J. Alloys Comp.*, 1999, vol. 282, p. 261.

9. Kim. D.-M., Jang, K.-J., and Lee, J.-Y., *J. Alloys Comp.*, 1999, vol. 293-295, p. 583.

10. Ghoi, W.-K., Yamataka, K., Zhang, S.G., Inoue, H., and Iwakura, C., *J. Electrochem. Soc.*, 1999, vol. 146, p. 46.

11. Zotov, T.A., Verbetskii, V.N., Safonova, T.Ya., and Petrii, O.A., Abstracts of Papers, *Proc. Int. Symp. on Metal Hydrogen Systems: Fundamentals and Applications, Noosa (Australia), 2000*, p. 55.

12. Zotov, T.A., Petrii, O.A., and Verbetskii, V.N., *NATO Sci. Ser. II Math. Phys. Chem.*, 2002, vol. 82, p. 229.

13. Zotov, T.A., Verbetskii, V.N., Safonova, T.Ya., and Petrii, O.A., *J. Solid State Electrochem.,* 2003, vol. 7, p. 645.

14. Zotov, T.A., Verbetskii, V.N., Petrii, O.A., and Safonova, T.Ya., *NATO Sci. Ser. II Math. Phys. Chem.*, 2004, vol. 172, p. 569.

15. Perii, O.A., Gogichadze, I.L., and Vasina, S.Ya., *Trudy VII Simp. "Dvoinoi sloi i adsorbtsiya na tverdykh elektrodakh*" (Proc. VIII Symp. on Double Layer and Adsorption at Solid Electrodes), Tartu: Tartus. Gos. Univ., 1985, p. 213.

16. Nakano, H. and Wakao, S., *J. Alloys Comp.*, 1995, vol. 231, p. 587.

17. Nakano, H., Wakao, S., and Shimizu, T., *J. Alloys Comp.,* 1997, vol. 253-254, p. 609.

18. Wakao, S. and Yonemura, Y., *J. Less-Common Met.*, 1983, vol. 89, p. 481.